Citation for published version:
Chereau, E, Dubrovskii, VG, Grégoire, G, Avit, G, Staudinger, P, Schmid, H, Bougerol, C, Coulon, PM, Shields, PA, Trassoudaine, A, Gil, E & LaPierre, RR 2023, 'Importance of As and Ga Balance in Achieving Long GaAs Nanowires by Selective Area Epitaxy', *Crystal Growth and Design*, vol. 23, no. 6, pp. 4401-4409. https://doi.org/10.1021/acs.cgd.3c00172

DOI:
10.1021/acs.cgd.3c00172

Publication date:
2023

Document Version
Peer reviewed version

Link to publication

This document is the Accepted Manuscript version of a Published Work that appeared in final form in Crystal Growth and Design, copyright © American Chemical Society after peer review and technical editing by the publisher. To access the final edited and published work see https://pubs.acs.org/doi/10.1021/acs.cgd.3c00172

University of Bath

Alternative formats
If you require this document in an alternative format, please contact:
openaccess@bath.ac.uk

General rights
Copyright and moral rights for the publications made accessible in the public portal are retained by the authors and/or other copyright owners and it is a condition of accessing publications that users recognise and abide by the legal requirements associated with these rights.

Take down policy
If you believe that this document breaches copyright please contact us providing details, and we will remove access to the work immediately and investigate your claim.

Download date: 28. May. 2024

The importance of As and Ga balance in achieving long GaAs nanowires by selective area epitaxy

Emmanuel Chereau[1], Vladimir G. Dubrovskii[2], Gabin Grégoire[1], Geoffrey Avit[1], Philipp Staudinger[3], Heinz Schmid[3], Catherine Bougerol[4], Pierre-Marie Coulon[5,6], Philip A. Shields[6], Agnès Trassoudaine[1], Evelyne Gil[1], Ray R. LaPierre[7], Yamina André[1]

[1]Université Clermont Auvergne, CNRS, Clermont Auvergne INP, Institut Pascal, F-63000 Clermont-Ferrand, France
[2]Faculty of Physics, St. Petersburg State University, Universitetskaya Embankment 13B, 199034 St. Petersburg, Russia
[3]IBM Research Europe - Zürich, Saumerstrasse 4, 8803 Rüschlikon, Switzerland
[4]Université Grenoble Alpes, CNRS, Institut Neel, 38000 Grenoble, France
[5]Université Côte d'Azur, CNRS, CRHEA, Rue Bernard Gregory, 06560 Valbonne, France
[6]Centre for Nanoscience and Nanotechnology & Department of Electronic and Electrical Engineering, University of Bath, Bath, BA2 7AY, United Kingdom
[7]Department of Engineering Physics, McMaster University, Hamilton, Ontario Canada, L8S4L7

Abstract

We report on the selective area growth (SAG) of GaAs nanowires (NWs) by the catalyst-free vapor-solid mechanism. Well-ordered GaAs NWs were grown on GaAs(111)B substrates patterned with a dielectric mask using hydride vapor phase epitaxy (HVPE). GaAs NWs were grown along the <111>B direction with perfect hexagonal shape when the holes opening diameter in SiN_x or SiO_x mask was varied from 80 nm to 340 nm. The impact of growth conditions and the hole size on the NW lengths and growth rates was investigated. A saturation of the NW lengths was observed at high partial pressures of As_4, explained by the presence of As trimers on the (111)B surface at the NW top surface. By decreasing As_4 partial pressure and decreasing the hole size, high aspect ratio NWs were obtained. The longest and thinnest NWs grew faster than a two-dimensional layer under the same conditions, which strongly suggests that surface diffusion of Ga adatoms from the NW sidewalls to their top contributes to the resulting axial growth rate. These findings were supported

by a dedicated model. The study highlights the capability of the HVPE process to grow high aspect ratio GaAs NW arrays with high selectivity.

Introduction

Over the last decades, III-V semiconductor nanowires (NWs) have attracted much attention due to their unique physical properties and potential applications in nanoelectronics and optoelectronics. Amongst III-V semiconductors, GaAs has significant merits due to a direct band gap and high electron mobility, leading to excellent optical and electronic properties[1]. A wide range of GaAs NWs based devices have been built such as solar cells[2,3], lasers[4], photodetectors[5], field-effect transistors[6] and light emitting diodes[7].

Several methods have been developed to grow GaAs NWs with a high material quality. To date, the most common method is the vapor-liquid-solid (VLS) growth promoted by a metal catalyst [8,9]. High quality GaAs NWs have been obtained by Au-assisted molecular beam epitaxy (MBE)[10] and metalorganic vapor phase epitaxy (MOVPE)[11]. However, the foreign Au catalyst can contaminate the NWs by introducing deep level recombination centers, which significantly degrades the electrical and optical properties of GaAs material[12,13]. Consequently, much effort has been put on growing Au-free GaAs NWs in the self-catalyzed VLS approach, in which the Au catalyst is replaced by Ga[14–17]. The random arrangement and size of the NW growth seeds on unpatterned substrates lead to inhomogeneity of the NW ensembles in terms of their diameter, length, position and growth direction. This randomness induces inhomogeneities of the electronic and optical properties, making the fabrication of devices very difficult. Selective area growth (SAG), which implements the NW growth in lithographically defined openings in a dielectric mask layer, is a powerful solution to fabricate highly regular, large-scale NW arrays with improved properties[18]. In point of fact, SAG of GaAs NWs on Si(111) and GaAs(111)B substrates has been demonstrated by MBE[19,20] and MOVPE[21–24] techniques.

Hydride vapor phase epitaxy (HVPE) is another process to grow III-V structures, from V-hydride and III-chloride gaseous precursors. HVPE is known for its perfect intrinsic selectivity due to the low sticking coefficient of the III-chloride precursors on dielectric masks[25]. This technique has demonstrated exceptional results for the Au-assisted growth of ultra-thin (10 nm diameter), pure

zincblende (ZB) GaAs NWs with a record growth rate[26]. While SAG by HVPE has been successfully used to grow InAs NWs and III-nitride nanorods[27–29], no such in-depth study of SAG of GaAs NW arrays has been achieved by this technique. Consequently, here we study the features of SAG of GaAs NWs using SiN_x and SiO_x patterned GaAs (111)B substrates by HVPE. We investigate the growth process and the NW morphology versus the deposition conditions and template geometry to reveal the steps and mechanisms involved in GaAs SAG by HVPE. Peculiar features are found depending on the As_4 partial pressure: suppression of the axial growth of NWs at high As_4 partial pressures, and efficient growth of high aspect ratio NWs at reduced As_4 supply due to surface diffusion of Ga adatoms enhancing the axial NW growth rate above the two-dimensional (2D) growth rate. A kinetic growth model is developed to explain and quantify these effects. Overall, this study demonstrates the feasibility and reveals the optimal growth conditions for uniform selective GaAs NWs with high aspect ratios by HVPE.

▪ Experimental

SAG of GaAs NWs was performed on (111)B-oriented GaAs substrates. A 35 nm thick SiN_x layer, deposited by plasma-enhanced chemical vapor deposition and patterned by displacement Talbot lithography (DTL) into periodic hexagonal arrays of circular holes with a diameter of 340 nm and a pitch of 1 µm, was used as a mask. More details of DTL can be found in Ref.[30]. In some experiments, the substrate was patterned by electron beam lithography and the mask was changed to SiO_x. In this case, the hole diameter was 80 nm and the pitch was varied between 1 µm and 2 µm. Samples were loaded into a hot-wall HVPE reactor working at atmospheric pressure, with H_2 as a carrier gas. The reactor is divided into three zones, heated by a six-zone furnace. In the first zone, gaseous HCl reacted with a liquid Ga source at 760 °C to form the GaCl precursor. AsH_3 gas was introduced in the downstream central zone, heated to a higher temperature to ensure homogeneous mixing of the gas phase. The hot temperature zone also reduces parasitic nucleation upstream of the substrate, since the growth reactions involving chloride molecules are exothermic. After introduction into the hot-wall reactor, AsH_3 was totally decomposed into As_4/As_2 species with equilibrium concentrations. The substrate was placed in the downstream growth zone, which was kept at a lower temperature compared to the central zone. The substrate surface interacted with the vapor phase composed of GaCl, As_4/As_2, H_2 and HCl species.

The partial pressures of GaCl, HCl, As_4 and As_2 above the substrate were calculated as a function of the input flows of AsH_3, HCl (above the liquid Ga source) and H_2, considering the kinetics of decomposition of AsH_3 into As_4 and As_2, the thermodynamic equilibrium constants of the intermediate chemical reactions, and the temperature gradient along the reactor. The partial pressure of As_4, noted P_{As4}, was varied from 3.0×10^{-4} atm to 1.0×10^{-3} atm, while the partial pressure of GaCl, noted P_{GaCl}, was varied from 7.8×10^{-4} atm to 4.7×10^{-3} atm. The samples were heated to 742 °C for GaAs deposition in all cases. In order to compare the NW axial growth rate with the 2D growth rate, 2D GaAs layers were grown on unpatterned GaAs (111)B substrates in the same growth run. The atomic III/V ratios were calculated for each growth run as

$$\frac{I_3}{I_5} = \frac{1}{4}\frac{P_{Gacl}}{P_{As_4}}, \quad (1)$$

Each As_4 molecule brings four As atoms to the surface. Note that at our growth temperature the partial pressure of As_4 is a hundred times larger than that of As_2.

The morphology of as-grown NWs was studied using a Carl Zeiss Supra scanning electron microscope (SEM) with an acceleration voltage of 3 kV. NWs length and diameter were deduced from the SEM images. The diameter for tapered NWs was measured at the top just below the tapered section. The crystal structure was studied using a FEI-TECNAI transmission electron microscope (TEM) with an acceleration voltage of 200 kV.

▪ Results and discussion

The effect of the growth time on the NW morphology was investigated with the aim of growing long NWs. In these growth experiments, the partial pressures P_{As4} and P_{GaCl} were fixed at 1.0×10^{-3} atm and 1.6×10^{-3} atm, respectively, yielding a III/V ratio of 0.4. The opening diameter was 340 nm and the pitch was 1 µm. The growth time was varied between 5 min and 20 min. Figure 1a shows the schematics of SAG on patterned SiN_x/GaAs(111)B substrates. Figure 1b gives the measured evolution of the mean NW length and diameter given in Figure 1c-d .

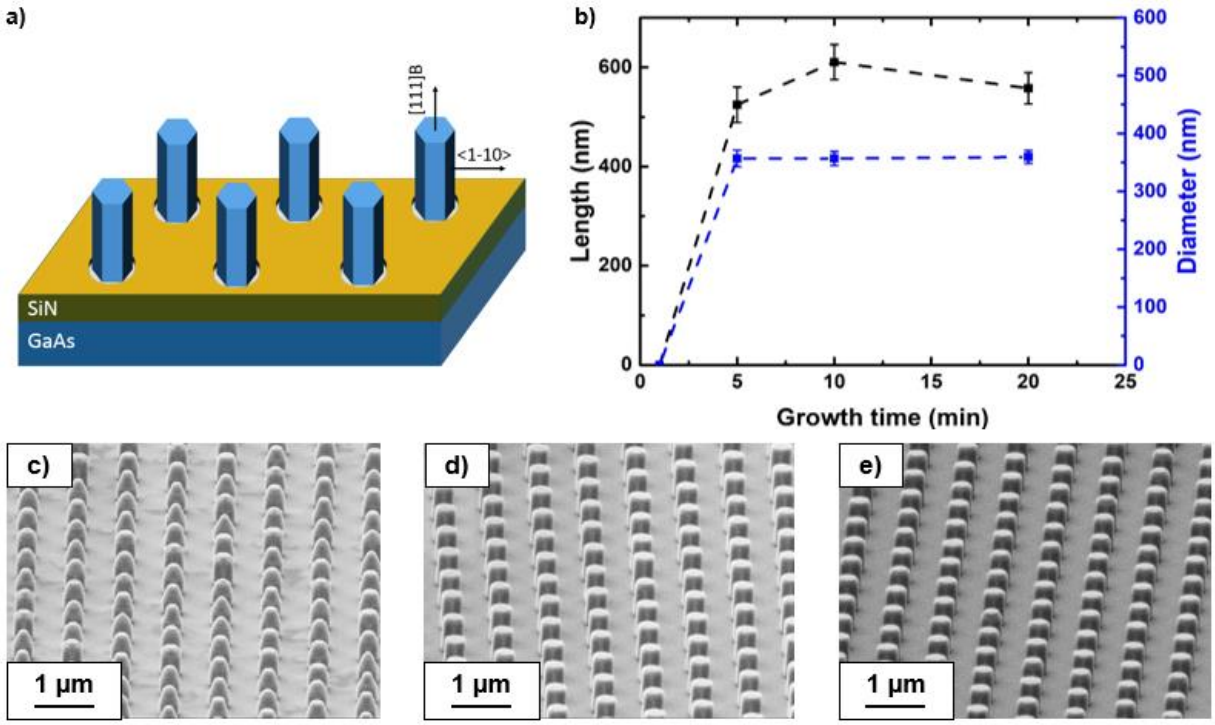

Figure 1. a) Schematic representation of SAG of GaAs NWs on patterned SiN_x/GaAs(111)B substrates by HVPE. b) Measured NW length and diameter as a function of the growth time, deduced from the tilted-view SEM images of GaAs NWs grown for different times: c) 5 min, d) 10 min and e) 20 min. For a growth time of 1 min, no growth was observed. Lines in b) are guides for the eye.

As expected, the growth is perfectly selective due to the low adsorption of chloride precursors on the mask. The NW growth kinetics exhibits the unusual non-linear behavior shown in Figure 1b. After 1 min of GaAs deposition, no NW growth above the mask surface was observed, revealing an incubation time required for nucleation of the NW seeds in the openings of SiN_x layer and filling the openings with GaAs. The processes occurring in the incubation stage include nucleation of GaAs island, most probably at the edge of the pinhole, its lateral extension and further overgrowth until the NW emerges above the mask layer. For long GaAs NWs studied in this work, the incubation stage results in a delay of NW growth above the mask for a certain time, which equals 1 min on average according to the data. The SEM images reveal that the NWs reach their maximum length of about 550 nm after only 5 min of GaAs deposition. The NWs shown in Figure 1c are not perfectly faceted and exhibit a tapered morphology. After 10 min and 20 min of GaAs deposition, the NWs have uniform diameter from base to top, with typical hexagonal cross-section restricted by the {-110} side facets, and the (111)B facet on top[31]. The radial growth rate on the {-110} side

facets, which consist of Ga-As rows, is usually very low over a wide range of HVPE conditions because of the low adsorption of GaCl on the {-110} surface. Hence, the radial growth rate of our NWs remains low whatever the growth conditions. The absence of any NW elongation after 5 min is attributed to a growth suppression effect on the (111)B top surface of the GaAs NWs as discussed below.

Two observations support the hypothesis of the NW growth suppression. First, HVPE growth is mainly governed by the adsorption-desorption kinetics of As and GaCl species and the dechlorination rate of the adsorbed AsGaCl species at a given surface[32]. The axial growth rate of NWs should equal at least the growth rate of a 2D layer under the same growth conditions (growth temperature and vapor phase composition), which is not the case here. Indeed, the measured 2D growth rate on the GaAs (111)B surface in these conditions is 305 nm/min, whereas the NWs axial growth rate before the growth suppression is only about 100 nm/min. In addition, no growth suppression effect on 2D GaAs (111)B surface is observed under the investigated experimental conditions. This shows that the growth suppression is indeed specific for SAG of GaAs NWs on patterned substrates.

To elucidate the origin of the NW growth suppression, we grew GaAs NWs on patterned SiN_x/GaAs(111)B substrates for 10 min at a fixed temperature of 742 °C under different partial pressures of P_{GaCl} and P_{As4}. The opening diameter was 340 nm and the pitch was 1 µm, as in Figure 1. Figure 2a shows the effect of P_{GaCl} variation at a constant P_{As4} of 1.0×10^{-3} atm, while Figure 2b shows the effect of P_{As4} variation at a constant P_{GaCl} of 1.6×10^{-3} atm. According to Figure 2a, the NW diameter increases with P_{GaCl}. This effect has already been observed for HVPE growth of GaAs stripes[33], and is explained by an increase of Ga adatom concentration on the sidewall surfaces. Different radial growth rates of NWs lead to a change in the NW morphology. At low P_{GaCl}, the top part of the NWs is tapered because the intrinsic growth rate of the (111)B facet is greater than the growth rate of the lateral facets. At high P_{GaCl}, the opposite occurs, the top facet clearly appears resulting in untapered NW morphology. However, the P_{GaCl} value does not have any significant influence on the NW length at $P_{As4}=1.0\times10^{-3}$ atm.

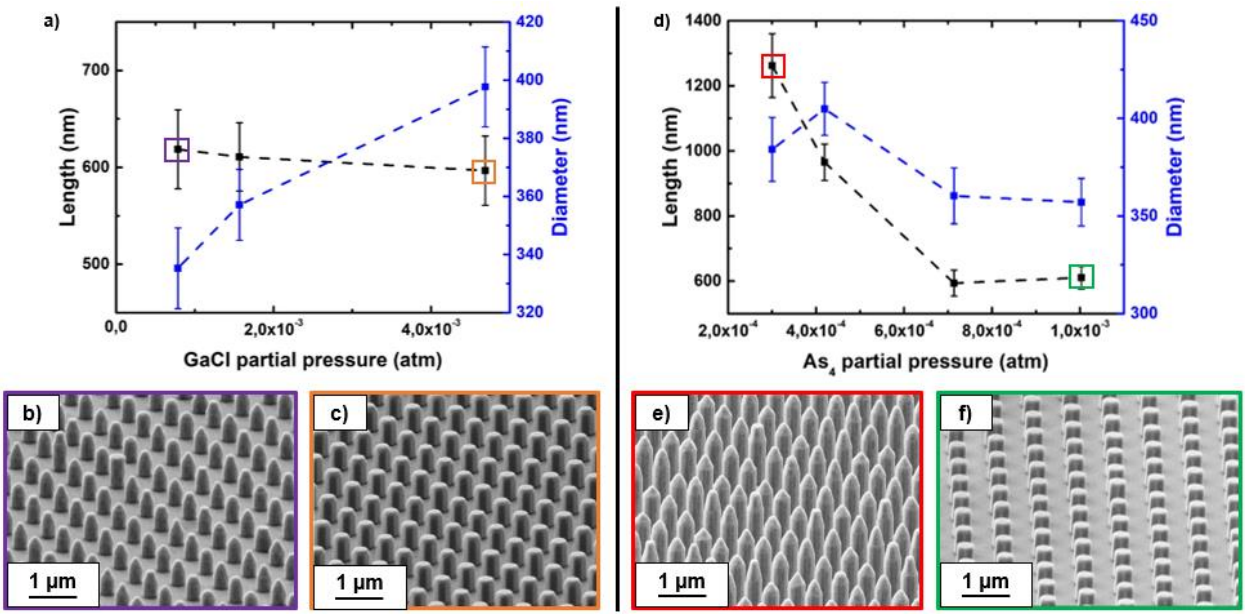

Figure 2. SAG GaAs NWs on patterned SiN_x/GaAs(111)B substrates with 340 nm hole diameter, grown for 10 min. a) NW length and diameter as a function of P_{GaCl} at a fixed P_{As4} of 1.0 x 10^{-3} atm. Tilted-view SEM images of GaAs NWs grown at different P_{GaCl}: b) 7.8×10^{-4} atm and c) 4.7×10^{-3} atm. D) NW length and diameter as a function of P_{As4} at a fixed P_{GaCl} of 1.6×10^{-3} atm. Tilted-view SEM images of GaAs NWs grown at different P_{As4}: e) 3.0×10^{-4} atm and f) 1.0×10^{-3} atm. The regimes yielding the maximum and minimum NW lengths and aspect ratios are highlighted in panels a) and d). Lines in a) and d) are guides for the eye.

According to Figure 2d, the P_{As4} value has a significant impact on the NW length, which strongly decreases for higher P_{As4}. The longest NWs grown at the lowest P_{As4} of 3.0×10^{-4} atm are tapered at the top, as seen in Figure 2e, while the shortest NWs grown at the highest P_{As4} of 1.0×10^{-3} atm are untapered. This should be associated with a higher axial growth rate of NWs grown at a lower P_{As4} and the absence of the growth suppression. The length of these NWs reaches 1262 nm after 10 min of growth, while the length of NWs grown at $P_{As4}=1.0\times10^{-3}$ atm is only 611 nm. These short NWs should have stopped elongating after 5 min of growth, as we saw earlier in Figure 1. After that, their tops have been modified by the radial growth to resume the untapered shape, as in Figure 1.

These data clearly show the importance of the P_{As4} value for obtaining long GaAs NWs in SAG by HVPE. Longer NWs can only be grown at low P_{As4} yielding high III/V ratios according to Eq. (1). According to Refs. [31,34–39], the growth of the (111)B top facet of GaAs NWs can be suppressed by stable As trimers when the As flux onto the NWs is too high, which suppresses the axial NW

growth under very As-rich conditions. For NWs grown at the highest P_{As4} of 1.0×10^{-3} atm (Figure 2f), the NW length has saturated at an early stage and hence the top facets of these NWs are fully covered with As trimers. No further growth can occur on such surfaces[40,41]. For NWs grown at lower P_{As4}, the top (111)B facets can be passivated only partly by As trimers or be completely free of As trimers. The axial growth then occurs on the parts of (111)B surface free from As trimers, or on the whole top facet in the absence of As trimers. This effect will be elaborated further in the modeling section of this work. Overall, the passivation of (111)B top facets of our GaAs NWs by As trimers under the excessive As input is suggested to be the reason for the suppression of the NW axial growth far below the 2D level. A higher As input onto the top facets of SAG NWs on the patterned substrates compared to 2D layers on unpatterned substrates is expected to be due to additional As_4 species desorbed from the inert mask and NW sidewalls. Therefore, the III/V ratios calculated from the partial pressures provide only the nominal values, while the actual ratio of atomic fluxes impinging on the NW tops may correspond to more As-rich growth conditions.

It is interesting to note that the NWs grown at low P_{As4} exhibit twelve side facets which belong to the two six-fold families equivalent to {-110} and {11-2}facets[10,40–44], as shown in the insert of Figure 3a. There are two possible explanations for such a faceting. The NWs may either nucleate with twelve facets initially and then keep this shape due to the equivalent growth rates on both types of facets, or they may nucleate with the energetically preferred six facets and the other facets appear in a later stage for kinetic reasons. If the NWs nucleate with twelve facets, the transition to a hexagonal shape restricted by six {-110} facets, as for NWs grown at higher P_{As4}, may occur by the elimination of the {11-2} facets. For wurtzite (WZ) GaAs NWs, the results of Ref.[45] show that the strong binding site found in calculations for GaAs pairs on the {11-20} facets may facilitate nucleation on these sidewalls. Consequently, for NWs with both facet families coexisting, the {11-20} facets may grow out and eventually disappear. Similar behavior may occur in GaAs NWs with predominantly zincblende (ZB) crystal phase, as in our case.

The extreme growth regimes yielding the NWs shown in Figures 2e and f result in very different NW morphologies. The crystal structure of these NWs was characterized by TEM. The results are shown in Figure 3a for a representative NW grown at a low P_{As4} of 3.0×10^{-4} atm, and in Figure 3b for a representative NW grown at a high P_{As4} of 1.0×10^{-3} atm. No significant difference in the crystal quality is observed between the two NWs. Both growth conditions yield GaAs NWs with a

high density of random stacking faults related to the ZB/WZ polytypism. This polytypism is commonly observed during growth of GaAs NWs along the <111B> direction[46–51]. The effect is attributed to a small difference in the internal formation energies of the two phases, which comes mainly from the electrostatic interaction between the third-nearest-neighbor atoms[46–48].

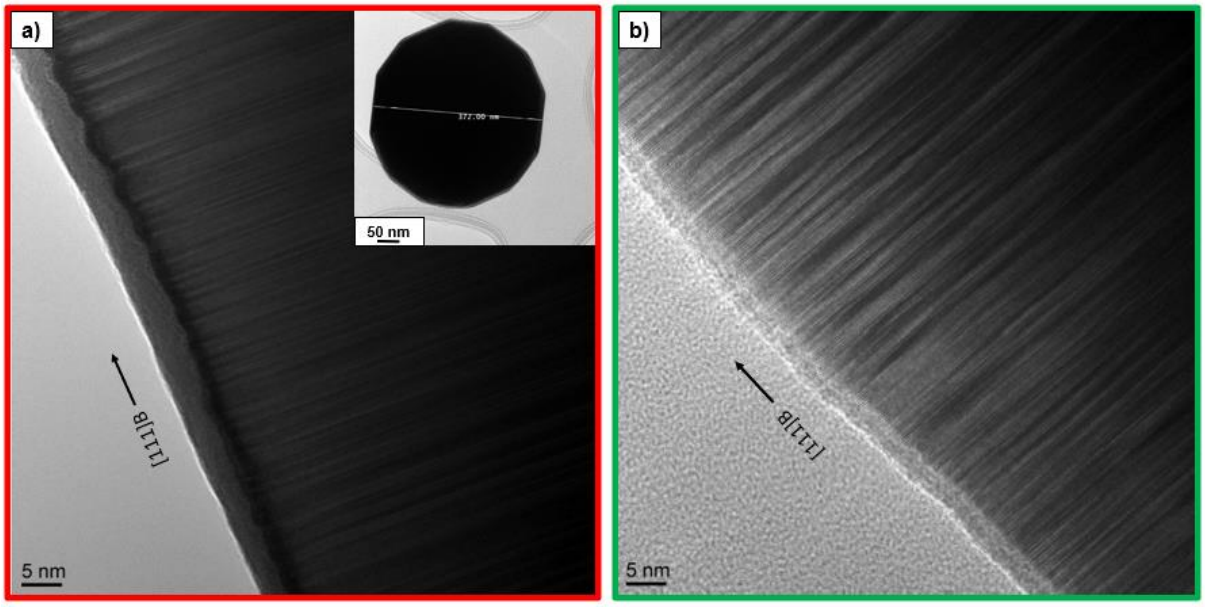

Figure 3. HR-TEM images of GaAs NWs grown on patterned SiN_x/GaAs (111)B substrates with 340 nm hole diameter at P_{As4} of a) 3.0×10^{-4} atm and b) 1.0×10^{-3} atm. The shell present on the NWs is an oxide layer. The incident electron beam was along to <1-10>. The inset in panel (a) is a TEM image along the [111]B direction showing the twelve side facets.

In order to confirm that the NW axial growth is not suppressed at low P_{As4}, we performed the SAG of GaAs NWs on patterned SiN_x/GaAs (111)B substrates with 340 nm hole diameter using two different values of P_{As4} of 3.0×10^{-4} atm and 4.2×10^{-4} atm for a longer time of 30 min. Figure 4 shows the SEM images of these NWs. The NW axial growth was still suppressed at $P_{As4}=4.2\times10^{-4}$ atm, where the NW length was almost the same as that after 10 min of growth (Figure 2d), but not suppressed at $P_{As4}=3.0\times10^{-4}$ atm. The NWs shown in Figure 4b exhibit a length of 6800 nm and an aspect ratio of more than 17. Thus, the average axial growth rate of these NWs was 227 nm/min and is approaching, but still lower than the 2D growth rate on GaAs(111)B substrate of 249 nm/min.

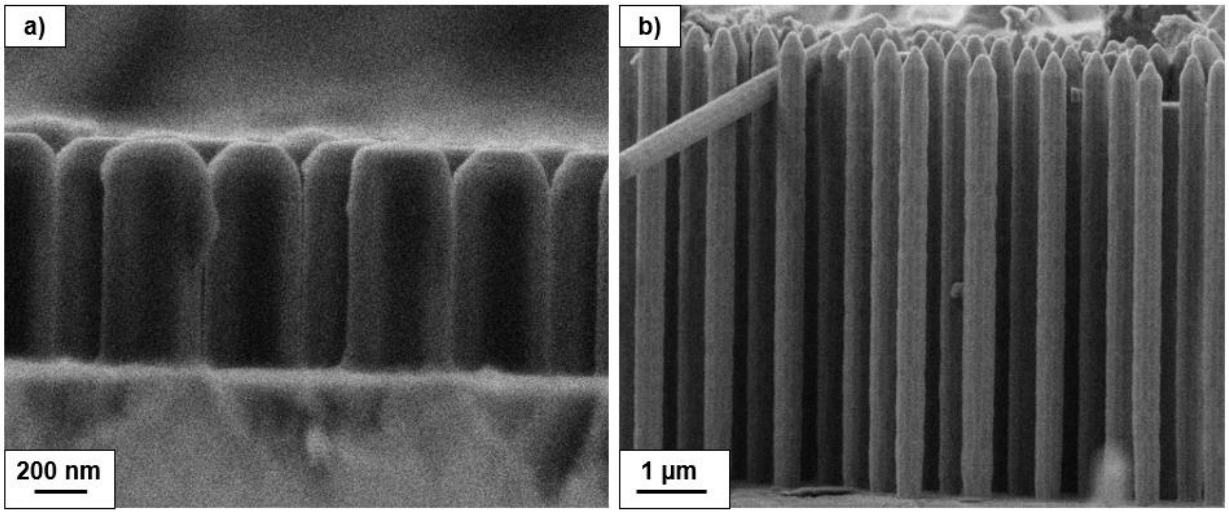

Figure 4. SEM images of GaAs NWs grown for 30 min on patterned SiN_x/GaAs (111)B substrates with 340 nm hole diameter using P_{As4} of a) 4.2×10^{-4} atm and b) 3.0×10^{-4} atm. The partial pressure P_{GaCl} was 1.6×10^{-3} atm in both cases.

The optimal growth conditions with the partial pressures $P_{As4}=3.0\times10^{-4}$ atm and $P_{GaCl}=1.6\times10^{-3}$ atm yielding the longest GaAs NWs on SiN_x/GaAs (111)B substrates with 340 nm hole diameter shown in Figure 4b, were used for the SAG of GaAs NWs on a different substrate. The dielectric mask was changed to SiO_x and the diameter of circular openings was reduced to 80 nm. Two different pitches of 1 µm and 2 µm were studied. The growth temperature was 742 °C, and the GaAs deposition time was 10 min. Figure 5 shows the SEM images of the NWs grown in arrays with different pitches. Perfect growth selectivity was observed, which is again explained by the negligible adsorption of the chloride precursors on the dielectric mask regardless of its chemical composition. Finally, the average axial growth rate of these NWs exceeded 550 nm/min, which is 2.2 times larger than the 2D growth rate of 249 nm/min. The NW length reached 5640 nm after only 10 min of GaAs deposition. With the NW diameter of 144 nm, this yields a record aspect ratio of 39. This result is remarkable for catalyst-free SAG III-V NWs in general.

Assuming that the axial NW growth is controlled by the Ga transport under As-rich conditions as discussed above, three different Ga fluxes should be considered[52]: (i) the impingement flux arriving onto the NW top directly from vapor, (ii) diffusion flux of Ga adatoms from the NW sidewalls to the top, and (iii) diffusion flux of Ga adatoms from the mask surface to the NW top[52]. The impingement flux (i) is identical for NWs and 2D layers because HVPE growth of GaAs is not

limited by the mass transfer. The diffusion flux from the mask (iii) should be absent due to the negligible adsorption of chloride precursors on the mask. Therefore, the only reason for the observed increase of the NW axial growth rate above the 2D level is the diffusion flux of Ga adatoms from the NW sidewalls (ii), which has never been considered in HVPE growth.

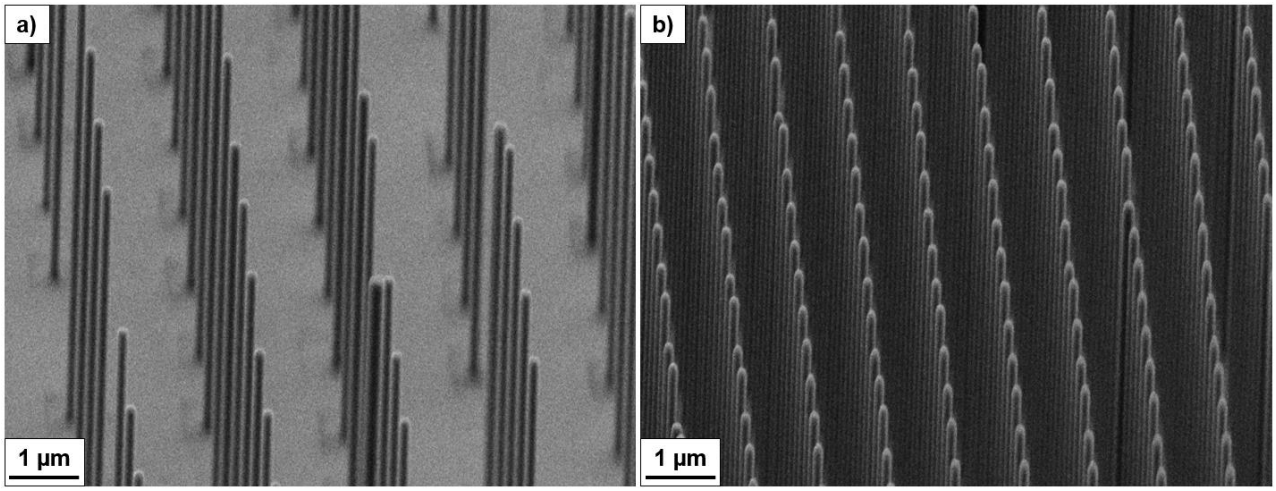

Figure 5. Tilted-view SEM images of GaAs NWs grown for 10 min on patterned SiO_x/GaAs(111)B substrates with 80 nm hole diameter and two different pitches of a) 2 µm and b) 1 µm. The partial pressures of precursors were fixed at $P_{GaCl}=1.6\times10^{-3}$ atm and $P_{As4}=3.0\times10^{-4}$ atm.

▪ Growth model

In growth modeling, we consider two effects which greatly influence the morphology of SAG GaAs NWs in the HVPE technique as discussed above. The model deals with the average values of the NW length and radius, neglecting statistical fluctuations and size distributions in the NW ensemble. First, we account for the axial growth suppression by As trimers under highly As-rich conditions at the NW top, which reduces the axial growth rate below the 2D level. Second, we introduce the possibility for surface diffusion of Ga adatoms from the NW sidewalls to the top, which can enhance the axial growth rate with respect to the 2D level. The model is illustrated in Figure 6a. Neglecting the radial growth in the first approximation by taking an average value for the NW radius R throughout the growth run ($R = (R_{hole} + R_f)/2$, where R_{hole} is the hole radius

and R_f is the measured NW radius after growth), the total change of the NW volume with time t is presented as

$$\pi R^2 \frac{dL}{dt} = \left[v_{2D}^{(111)B} \pi R^2 + v_{2D}^{f} 2\pi R \Lambda_3\right] \frac{S}{S_0}. \quad (2)$$

Here, L is the NW length above the mask surface, $v_{2D}^{(111)B}$ and v_{2D}^{f} are the 2D growth rates on the top (111)B facet and on the NW sidewall facets, respectively, Λ_3 is the Ga diffusion length on the NW sidewalls (labelled "3") and S/S_0 is the fraction of the top (111)B facet free from As trimers which suppress the axial NW growth. This fraction can equivalently be presented as $S/S_0 = 1 - \theta_5$, where θ_5 is the surface coverage of (111)B facet by As trimers (labelled "5"). The first bracket term describes the direct impingement and desorption of Ga atoms on the top facet, while the second bracket term gives the diffusion flux of Ga adatoms from the NW sidewalls to its top. From Eq. (2), the NW axial growth rate is given by

$$\frac{dL}{dt} = v_{2D}\left(1 + \frac{2\lambda_3}{R}\right)(1 - \theta_5), \quad (3)$$

with the effective diffusion length of Ga adatoms $\lambda_3 = \Lambda_3 \, v_{2D}^{f} / v_{2D}^{(111)B}$, where we write v_{2D} instead of $v_{2D}^{(111)B}$ for brevity. Clearly, the diffusion-induced contribution $2\lambda_3/R$ increases the NW growth rate above the 2D level, while the growth suppression effect on the NW top facet at $\theta_5 > 0$ decreases the NW growth rate below the 2D level.

The coverage of the top NW facet by As trimers is modeled using the simplest form of the Kolmogorov model[53]

$$\theta_5 = 1 - e^{-(t - t_{inc})/\tau_5}. \quad (4)$$

Here, $t_{inc} = 1$ min is the incubation time for NW growth above the mask surface as deduced from the growth experiments, and τ_5 is the characteristic time for forming As trimers on the top NW facet. Using this exponential dependence in Eq. (3) and integrating it with the initial condition $L(t = t_{inc}) = 0$, we obtain

$$L = v_{2D}\left(1 + \frac{2\lambda_3}{R}\right)\tau_5\left[1 - e^{-(t - t_{inc})/\tau_5)}\right]. \quad (5)$$

At $(t - t_{inc})/\tau_5 \gg 1$, corresponding to the full coverage of the top facet by As trimers ($\theta_5 \to 1$), the NW length saturates to a constant:

$$L \to v_{2D}\left(1 + \frac{2\lambda_3}{R}\right)\tau_5. \quad (6)$$

On the other hand, at $\tau_5 \to \infty$, corresponding to the absence of any As trimers at the NW top under effectively As-poor conditions, the NW length increases linearly with time:

$$L = v_{2D}\left(1 + \frac{2\lambda_3}{R}\right)(t - t_{inc}). \quad (7)$$

This is the usual law of NW elongation enhanced by surface diffusion above v_{2D}, as in Refs.[52,54]. The characteristic time of forming As trimers is expected to be shorter for lower III/V ratios I_3/I_5, corresponding to more As-rich conditions. The III/V ratios deduced from the partial pressures of GaCl and As_4 give only the nominal values above the substrate. The actual atomic III/V flux ratio on the NW top may be different. Nonetheless, lower I_3/I_5 ratios calculated from the partial pressure ratio should correspond to lower atomic III/V flux ratios at the NW top. The III/V balance on the NW top is also changed by the additional Ga adatoms diffusing from the NW sidewalls. It may be assumed that

$$\tau_5 = \tau_0 \frac{I_3}{I_5}\left(1 + \frac{2\lambda_3}{R}\right), \quad (8)$$

meaning that τ_5 is simply proportional to the effective atomic III/V ratio at the NW top $(I_3/I_5)(1 + 2\lambda_3/R)$ which includes surface diffusion of Ga adatoms with a constant τ_0. The formation of As trimers should have a barrier character. Therefore, the linear dependence given by Eq. (8) is expected only in a certain range of effective atomic III/V ratio below a threshold value. Above the threshold, τ_5 should rapidly tend to infinity and the growth suppression effect disappears.

Table 1 summarizes the partial pressures P_{Gacl} and P_{As_4}, the I_3/I_5 ratios given by Eq. (1), the hole diameters D_{hole} and pitches P of the SAG templates, the GaAs deposition times t, the measured 2D growth rates on unpatterned GaAs(111)B substrates v_{2D}, the lengths L and the average radii R of GaAs NWs used for modeling. The last two columns show the fitting parameters of the model λ_3 and τ_5 for each datapoint. It is remarkable that the good fits to the data are obtained with the same diffusion length of Ga adatoms of 44 nm. This value is smaller than for GaAs NW growth by MBE at much lower temperatures (typically below 640 °C), where the reported values are in the range of several hundreds of nm[52,54]. On the other hand, this value is very close to 45 nm, reported for Ga diffusion length on the sidewalls of GaN NWs grown by MBE in a temperature range from 770 °C to 810 °C[55]. The Ga diffusion length generally depends on the As pressure of III/V flux ratio, as discussed, for example, in Refs. [56–58]. In our growth experiments, the partial pressures of group III and V precursors are varied over a limited range such that the I_3/I_5 ratio changes from

0.4 to 1.33. The actual ratio of Ga and As fluxes landing on the NWs may be affected by the desorbed growth species. In this limited range, a flux-independent diffusion length of Ga adatoms on the NW sidewalls is usually a good approximation, as noted, for example, in Ref. [55] for the Ga diffusion length on the sidewalls of self-induced GaN NWs. For NWs which have twelve side facets belonging to the {-110} and {11-2} families, the previous reports on the growth kinetics of ZB GaAs NWs[10,52,54] revealed very similar Ga diffusion lengths on these surfaces. Therefore, using a constant Ga diffusion length of 44 nm for any III/V ratio does not contradict the previous findings and is supported by the fits. The deduced value of the diffusion length is very small. This allows us to safely neglect any pitch-dependent Ga diffusion from the mask, because all Ga adatoms which may have diffused from the mask to the NW sidewalls will re-evaporate before reaching the NW top.

Table 1. Parameters of GaAs NWs grown in different SAG conditions.

P_{Gacl} (10^{-3} atm)	P_{As_4} (10^{-3} atm)	I_3/I_5	D_{hole} (nm)	P (μm)	t (min)	L (nm)	v_{2D} (nm/min)	R (nm)	λ_3 (nm)	τ_5 (min)
1.6	1.0	0.40	340	1	5	521	304.5	174	44	1.26
1.6	1.0	0.40	340	1	10	611	304.5	174	44	1.26
1.6	1.0	0.40	340	1	20	580	304.5	174	44	1.26
1.6	0.7	0.56	340	1	10	594	244.2	175	44	1.62
1.6	0.4	0.95	340	1	10	965	248.5	186	44	2.78
1.6	0.4	0.95	340	1	30	1041	248.5	186	44	2.78
1.6	0.3	1.33	340	1	10	1262	247.2	181	44	3.47
1.6	0.3	1.33	80	1	10	5575	247.2	60	44	∞
1.6	0.3	1.33	80	2	10	5640	247.2	56	44	∞

Figure 6b shows the fits obtained from Eq. (5) for the NW lengths with saturation at I_3/I_5 =0.4 and 0.95. The fits are obtained with different τ_5. As expected, the fitting value of τ_5 increases for larger I_3/I_5. Figure 6c shows the main result of the model. The GaAs NW lengths obtained in 10 min growth experiments under different III/V ratios and in differently sized holes are compared to the 2D growth rates on unpatterned GaAs(111)B under the same growth conditions and fitted by Eq. (5) using different τ_5. It is seen that the model reproduces very well the data, including the axial growth suppression by As trimers at low effective III/V ratios and the axial growth increase above the 2D level due to surface diffusion of Ga adatoms to the top of the thinnest NWs.

According to Table 1, the longest and thinnest NWs grown in 80 nm diameter holes in a SiO_x mask at the highest I_3/I_5 of 1.33 are modelled with $\tau_5 \to \infty$. The small radius of these NWs simultaneously circumvents the unwanted effect of As trimer accumulation at the NW top and increases the axial NW growth rate far above the 2D level by a more efficient surface diffusion of Ga adatoms. Finally, Figure 6d demonstrates the validity of our hypothesis on the linear scaling of the characteristic time τ_5 with $(I_3/I_5)(1 + 2\lambda_3/R)$ in the range where the growth suppression effect is present.

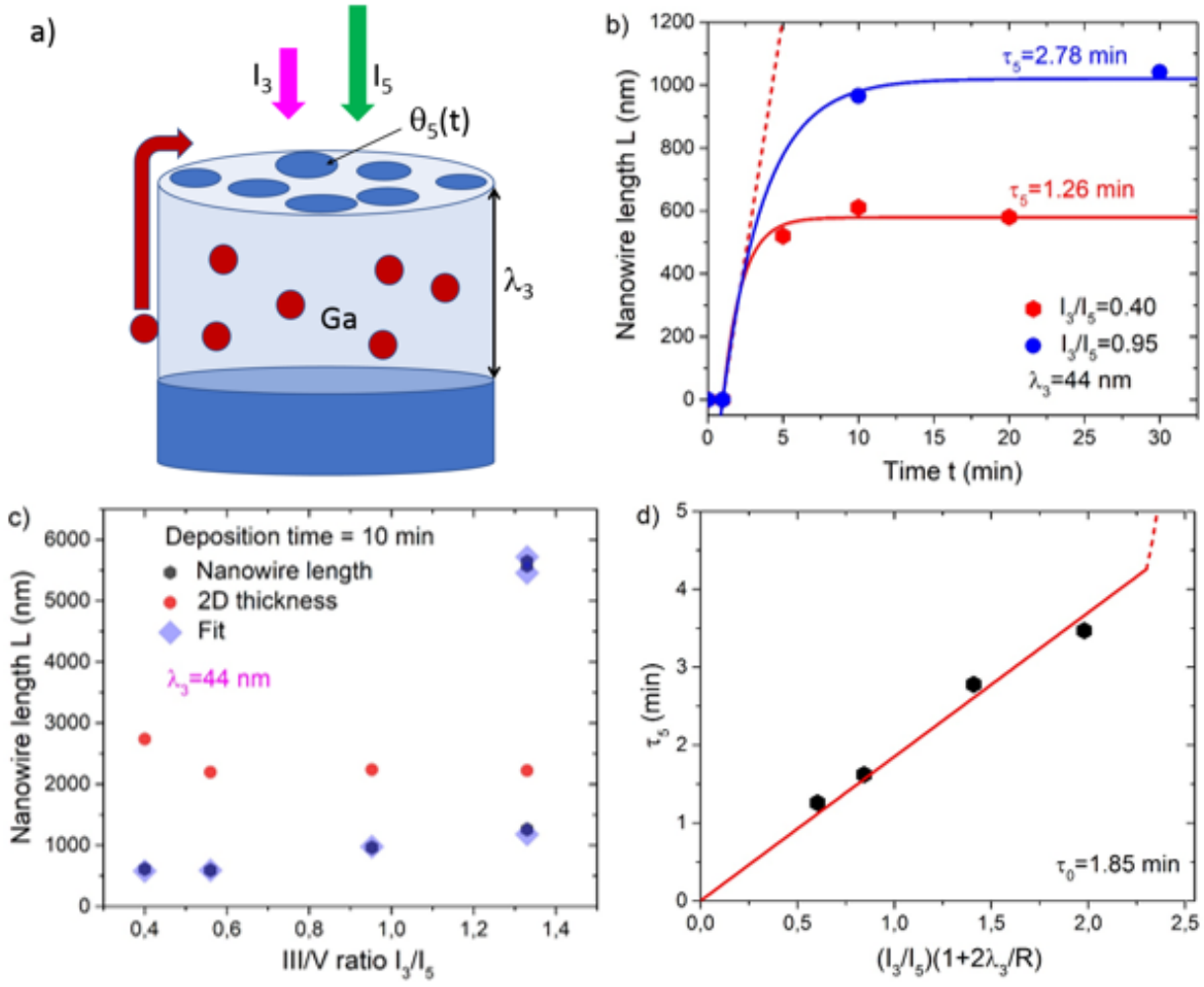

Figure 6. Illustration of the model in which the top (111)B NW facet is suppressed by As trimers with a time-dependent coverage $\theta_5(t)$. The effective diffusion length of Ga adatoms on the NW sidewalls equals λ_3. b) Lengths of GaAs NWs versus time at two different V/III ratios of 0.4 and 0.95 corresponding to the growth suppression by As trimers at the NW tops (symbols), fitted by the model with the parameters shown in the legend (lines). The dashed straight line corresponds to the 2D layer thickness on unpatterned GaAs (111)B substrate at $I_3/I_5 = 0.4$. c) Lengths of GaAs NWs after t=10 min, fitted by the model and compared to the 2D layer thickness. d) Linear increase

of the effective time τ_5 with the III/V input ratio. Dashed line shows a rapid increase of τ_5 for higher III/V input ratios.

▪ Conclusions

In conclusion, we demonstrated the SAG of GaAs NW arrays on GaAs(111)B substrates with excellent selectivity using the HVPE technique. The NW morphology was carefully investigated versus the growth conditions and template geometry. The TEM measurements confirmed the presence of stacking faults in NW structures. The growth study revealed the following insights into GaAs SAG. First, As-rich conditions are highly undesirable for SAG of GaAs NWs by HVPE due to the formation of As trimers which suppresses the axial NW growth. This effect was explained by As trimers forming on the top NW facet. Second, the highest aspect ratio GaAs NWs were obtained under reduced As pressures and using small 80 nm diameter holes. The optimal growth conditions for growing long NWs were promoted by surface diffusion of Ga adatoms from the NW sidewalls to the top. The effective diffusion length of Ga adatoms on the NW sidewalls was estimated at 44 nm at a growth temperature of 742 ^{o}C and resulted in an increase of the NW growth rate compared to the 2D growth rate by a factor of 2.2. The longest GaAs NWs reached a length of about 5600 nm within 10 min, resulting in a NW with an aspect ratio of about 50. Overall, SAG of GaAs NWs by HVPE provides a new platform for fabrication of NW arrays with record high aspect ratios, with the potential to be transferable to other III-V materials.

▪ Author information

Corresponding authors

*Emmanuel CHEREAU. Institut Pascal, 4 Avenue Blaise Pascal, 63178 Aubière Cedex. France.
E-mail: emmanuel.chereau@uca.fr

*Yamina ANDRE. Institut Pascal, 4 Avenue Blaise Pascal, 63178 Aubière Cedex. France.
E-mail: yamina.andre@uca.fr

*Evelyne GIL. Institut Pascal, 4 Avenue Blaise Pascal, 63178 Aubière Cedex. France.
E-mail: evelyne.gil@uca.fr

Author contributions

The manuscript was written through contributions of all authors. All authors have given approval to the final version of the manuscript.

Acknowledgements

This work was supported by Région Auvergne Rhône-Alpes; Pack ambition international NanoSpring DRV_PIP_2021-252_IP_NANOSPRING (https://www.auvergnerhonealpes.fr/77-logo.htm).

This work was supported by the International Research Center "Innovation Transportation and Production Systems" of the I-SITE CAP 20-25."

It was also funded by the program “Investissements d’avenir” of the French ANR agency, the French government IDEX-SITE initiative 16-µIDEX-0001 (CAP 20-25), the European Commission (Auvergne FEDER Funds), and the Region Auvergne in the framework of the LabEx IMobS3 (ANR-10-LABX-16-01).

The authors thank 2MAtech, Aubiere, France, for scanning electron microscopy measurements.

This work also received funding from the H2020 ERC POC project ENUF, grant number 790448.

VGD gratefully acknowledges financial support of St. Petersburg State University under the research grant No. 75746688.

RRL acknowledges the financial support of the Natural Sciences and Engineering Research Council of Canada from grants RGPIN-2018-04015 and RGPAS-2018-522624.

References

(1) Wolfe, C. M.; Stillman, G. E.; Lindley, W. T. Electron Mobility in High-Purity GaAs. *J. Appl. Phys.* **1970**, *41* (7), 3088–3091. https://doi.org/10.1063/1.1659368.

(2) Krogstrup, P.; Jørgensen, H. I.; Heiss, M.; Demichel, O.; Holm, J. V.; Aagesen, M.; Nygard, J.; Fontcuberta i Morral, A. Single-Nanowire Solar Cells beyond the Shockley–Queisser Limit. *Nat. Photonics* **2013**, *7* (4), 306–310. https://doi.org/10.1038/nphoton.2013.32.

(3) Åberg, I.; Vescovi, G.; Asoli, D.; Naseem, U.; Gilboy, J. P.; Sundvall, C.; Dahlgren, A.; Svensson, K. E.; Anttu, N.; Björk, M. T.; Samuelson, L. A GaAs Nanowire Array Solar Cell With 15.3% Efficiency at 1 Sun. *IEEE J. Photovolt.* **2016**, *6* (1), 185–190. https://doi.org/10.1109/JPHOTOV.2015.2484967.
(4) Saxena, D.; Mokkapati, S.; Parkinson, P.; Jiang, N.; Gao, Q.; Tan, H. H.; Jagadish, C. Optically Pumped Room-Temperature GaAs Nanowire Lasers. *Nat. Photonics* **2013**, *7* (12), 963–968. https://doi.org/10.1038/nphoton.2013.303.
(5) Dai, X.; Zhang, S.; Wang, Z.; Adamo, G.; Liu, H.; Huang, Y.; Couteau, C.; Soci, C. GaAs/AlGaAs Nanowire Photodetector. *Nano Lett.* **2014**, *14* (5), 2688–2693. https://doi.org/10.1021/nl5006004.
(6) Tomioka, K.; Yoshimura, M.; Fukui, T. A III–V Nanowire Channel on Silicon for High-Performance Vertical Transistors. *Nature* **2012**, *488* (7410), 189–192. https://doi.org/10.1038/nature11293.
(7) Tomioka, K.; Motohisa, J.; Hara, S.; Hiruma, K.; Fukui, T. GaAs/AlGaAs Core Multishell Nanowire-Based Light-Emitting Diodes on Si. *Nano Lett.* **2010**, *10* (5), 1639–1644. https://doi.org/10.1021/nl9041774.
(8) Wagner, R. S.; Ellis, W. C. Vapor-liquid-solid Mechanism of Single Crystal Growth. *Appl. Phys. Lett.* **1964**, *4* (5), 89–90. https://doi.org/10.1063/1.1753975.
(9) Duan, X.; Lieber, C. M. General Synthesis of Compound Semiconductor Nanowires. *Adv. Mater.* **2000**, *12* (4), 298–302. https://doi.org/10.1002/(SICI)1521-4095(200002)12:4<298::AID-ADMA298>3.0.CO;2-Y.
(10) Plante, M. C.; LaPierre, R. R. Control of GaAs Nanowire Morphology and Crystal Structure. *Nanotechnology* **2008**, *19* (49), 495603. https://doi.org/10.1088/0957-4484/19/49/495603.
(11) Joyce, H. J.; Gao, Q.; Tan, H. H.; Jagadish, C.; Kim, Y.; Fickenscher, M. A.; Perera, S.; Hoang, T. B.; Smith, L. M.; Jackson, H. E.; Yarrison-Rice, J. M.; Zhang, X.; Zou, J. High Purity GaAs Nanowires Free of Planar Defects: Growth and Characterization. *Adv. Funct. Mater.* **2008**, *18* (23), 3794–3800. https://doi.org/10.1002/adfm.200800625.
(12) Breuer, S.; Pfüller, C.; Flissikowski, T.; Brandt, O.; Grahn, H. T.; Geelhaar, L.; Riechert, H. Suitability of Au- and Self-Assisted GaAs Nanowires for Optoelectronic Applications. *Nano Lett.* **2011**, *11* (3), 1276–1279. https://doi.org/10.1021/nl104316t.
(13) Bar-Sadan, M.; Barthel, J.; Shtrikman, H.; Houben, L. Direct Imaging of Single Au Atoms Within GaAs Nanowires. *Nano Lett.* **2012**, *12* (5), 2352–2356. https://doi.org/10.1021/nl300314k.
(14) Ihn, S.-G.; Song, J.-I.; Kim, T.-W.; Leem, D.-S.; Lee, T.; Lee, S.-G.; Koh, E. K.; Song, K. Morphology- and Orientation-Controlled Gallium Arsenide Nanowires on Silicon Substrates. *Nano Lett.* **2007**, *7* (1), 39–44. https://doi.org/10.1021/nl0618795.
(15) Ambrosini, S.; Fanetti, M.; Grillo, V.; Franciosi, A.; Rubini, S. Vapor-Liquid-Solid and Vapor-Solid Growth of Self-Catalyzed GaAs Nanowires. *AIP Adv.* **2011**, *1* (4), 042142. https://doi.org/10.1063/1.3664133.
(16) Dong, Z.; André, Y.; Dubrovskii, V. G.; Bougerol, C.; Leroux, C.; Ramdani, M. R.; Monier, G.; Trassoudaine, A.; Castelluci, D.; Gil, E. Self-Catalyzed GaAs Nanowires on Silicon by Hydride Vapor Phase Epitaxy. *Nanotechnology* **2017**, *28* (12), 125602. https://doi.org/10.1088/1361-6528/aa5c6b.
(17) Panciera, F.; Baraissov, Z.; Patriarche, G.; Dubrovskii, V. G.; Glas, F.; Travers, L.; Mirsaidov, U.; Harmand, J.-C. Phase Selection in Self-Catalyzed GaAs Nanowires. *Nano Lett.* **2020**, *20* (3), 1669–1675. https://doi.org/10.1021/acs.nanolett.9b04808.
(18) Tomioka, K.; Ikejiri, K.; Tanaka, T.; Motohisa, J.; Hara, S.; Hiruma, K.; Fukui, T. Selective-Area Growth of III-V Nanowires and Their Applications. *J. Mater. Res.* **2011**, *26* (17), 2127–2141. https://doi.org/10.1557/jmr.2011.103.
(19) Yoshida, S.; Tamai, I.; Sato, T.; Hasegawa, H. Selective Molecular Beam Epitaxy Growth of GaAs Hexagonal Nanowire Networks on (111)B Patterned Substrates. *Jpn. J. Appl. Phys.* **2004**, *43* (4S), 2064. https://doi.org/10.1143/JJAP.43.2064.

(20) Dubrovskii, V. G.; Kim, W.; Piazza, V.; Güniat, L.; Fontcuberta i Morral, A. Simultaneous Selective Area Growth of Wurtzite and Zincblende Self-Catalyzed GaAs Nanowires on Silicon. *Nano Lett.* **2021**, *21* (7), 3139–3145. https://doi.org/10.1021/acs.nanolett.1c00349.
(21) Motohisa, J.; Noborisaka, J.; Takeda, J.; Inari, M.; Fukui, T. Catalyst-Free Selective-Area MOVPE of Semiconductor Nanowires on (111)B Oriented Substrates. *J. Cryst. Growth* **2004**, *272* (1), 180–185. https://doi.org/10.1016/j.jcrysgro.2004.08.118.
(22) Noborisaka, J.; Motohisa, J.; Fukui, T. Catalyst-Free Growth of GaAs Nanowires by Selective-Area Metalorganic Vapor-Phase Epitaxy. *Appl. Phys. Lett.* **2005**, *86* (21), 213102. https://doi.org/10.1063/1.1935038.
(23) Paetzelt, H.; Gottschalch, V.; Bauer, J.; Benndorf, G.; Wagner, G. Selective-Area Growth of GaAs and InAs Nanowires—Homo- and Heteroepitaxy Using SiNx Templates. *J. Cryst. Growth* **2008**, *310* (23), 5093–5097. https://doi.org/10.1016/j.jcrysgro.2008.06.065.
(24) Kim, H.; Ren, D.; Farrell, A. C.; Huffaker, D. L. Catalyst-Free Selective-Area Epitaxy of GaAs Nanowires by Metal-Organic Chemical Vapor Deposition Using Triethylgallium. *Nanotechnology* **2018**, *29* (8), 085601. https://doi.org/10.1088/1361-6528/aaa52e.
(25) Gil, E.; André, Y.; Cadoret, R.; Trassoudaine, A. 2 - Hydride Vapor Phase Epitaxy for Current III–V and Nitride Semiconductor Compound Issues. In *Handbook of Crystal Growth (Second Edition)*; Kuech, T. F., Ed.; Handbook of Crystal Growth; North-Holland: Boston, 2015; pp 51–93. https://doi.org/10.1016/B978-0-444-63304-0.00002-0.
(26) Gil, E.; Dubrovskii, V. G.; Avit, G.; André, Y.; Leroux, C.; Lekhal, K.; Grecenkov, J.; Trassoudaine, A.; Castelluci, D.; Monier, G.; Ramdani, R. M.; Robert-Goumet, C.; Bideux, L.; Harmand, J. C.; Glas, F. Record Pure Zincblende Phase in GaAs Nanowires down to 5 Nm in Radius. *Nano Lett.* **2014**, *14* (7), 3938–3944. https://doi.org/10.1021/nl501239h.
(27) Grégoire, G.; Zeghouane, M.; Goosney, C.; Goktas, N. I.; Staudinger, P.; Schmid, H.; Moselund, K. E.; Taliercio, T.; Tournié, E.; Trassoudaine, A.; Gil, E.; LaPierre, R. R.; André, Y. Selective Area Growth by Hydride Vapor Phase Epitaxy and Optical Properties of InAs Nanowire Arrays. *Cryst. Growth Des.* **2021**, *21* (9), 5158–5163. https://doi.org/10.1021/acs.cgd.1c00518.
(28) Avit, G.; Zeghouane, M.; André, Y.; Castelluci, D.; Gil, E.; Baé, S.-Y.; Amano, H.; Trassoudaine, A. Crystal Engineering by Tuning the Growth Kinetics of GaN 3-D Microstructures in SAG-HVPE. *CrystEngComm* **2018**, *20* (40), 6207–6213. https://doi.org/10.1039/C8CE01177J.
(29) Zeghouane, M.; Avit, G.; Cornelius, T. W.; Salomon, D.; André, Y.; Bougerol, C.; Taliercio, T.; Meguekam-Sado, A.; Ferret, P.; Castelluci, D.; Gil, E.; Tournié, E.; Thomas, O.; Trassoudaine, A. Selective Growth of Ordered Hexagonal InN Nanorods. *CrystEngComm* **2019**, *21* (16), 2702–2708. https://doi.org/10.1039/C9CE00161A.
(30) Coulon, P.-M.; Damilano, B.; Alloing, B.; Chausse, P.; Walde, S.; Enslin, J.; Armstrong, R.; Vézian, S.; Hagedorn, S.; Wernicke, T.; Massies, J.; Zúñiga-Pérez, J.; Weyers, M.; Kneissl, M.; Shields, P. A. Displacement Talbot Lithography for Nano-Engineering of III-Nitride Materials. *Microsyst. Nanoeng.* **2019**, *5* (1), 1–12. https://doi.org/10.1038/s41378-019-0101-2.
(31) Yeu, I. W.; Han, G.; Park, J.; Hwang, C. S.; Choi, J.-H. Theoretical Understanding of the Catalyst-Free Growth Mechanism of GaAs \textbackslashtextless111\textbackslashtextgreaterB Nanowires. *Appl. Surf. Sci.* **2019**, *497*, 143740. https://doi.org/10.1016/j.apsusc.2019.143740.
(32) Gil-Lafon, E.; Napierala, J.; Castelluci, D.; Pimpinelli, A.; Cadoret, R.; Gérard, B. Selective Growth of GaAs by HVPE: Keys for Accurate Control of the Growth Morphologies. *J. Cryst. Growth* **2001**, *222* (3), 482–496. https://doi.org/10.1016/S0022-0248(00)00961-1.
(33) Napierala, J.; Gil-Lafon, E.; Castelluci, D.; Pimpinelli, A.; Gérard, B. Control of the Growth Morphologies of GaAs Stripes Grown on Patterned Substrates by HVPE. *Opt. Mater.* **2001**, *17* (1), 315–318. https://doi.org/10.1016/S0925-3467(01)00097-0.

(34) *Facile Five-Step Heteroepitaxial Growth of GaAs Nanowires on Silicon Substrates and the Twin Formation Mechanism | ACS Nano*. https://pubs.acs.org/doi/10.1021/acsnano.5b07232 (accessed 2022-10-26).
(35) Biegelsen, D. K.; Bringans, R. D.; Northrup, J. E.; Swartz, L.-E. Reconstructions of GaAs(1\ifmmode\bar\else\textasciimacron\fi{} 1\ifmmode\bar\else\textasciimacron\fi{} 1\ifmmode\bar\else\textasciimacron\fi{}) Surfaces Observed by Scanning Tunneling Microscopy. *Phys. Rev. Lett.* **1990**, *65* (4), 452–455. https://doi.org/10.1103/PhysRevLett.65.452.
(36) Nishida, T.; Uwai, K.; Kobayashi, Y.; Kobayashi, N. K. N. Phase Diagram of GaAs (111)B Surface during Metal-Organic Chemical Vapor Deposition Measured by Surface Photo-Absorption. *Jpn. J. Appl. Phys.* **1995**, *34* (12R), 6326. https://doi.org/10.1143/JJAP.34.6326.
(37) Ohtake, A.; Nakamura, J.; Komura, T.; Hanada, T.; Yao, T.; Kuramochi, H.; Ozeki, M. Surface Structures of $\mathrm{GaAs}\mathrm{{}111\mathrm{}}A,B\ensuremath{-}(2\ifmmode\times\else\texttimes\fi{}2)$. *Phys. Rev. B* **2001**, *64* (4), 045318. https://doi.org/10.1103/PhysRevB.64.045318.
(38) Ikejiri, K.; Noborisaka, J.; Hara, S.; Motohisa, J.; Fukui, T. Mechanism of Catalyst-Free Growth of GaAs Nanowires by Selective Area MOVPE. *J. Cryst. Growth* **2007**, *298*, 616–619. https://doi.org/10.1016/j.jcrysgro.2006.10.179.
(39) Tomioka, K.; Ikejiri, K.; Tanaka, T.; Motohisa, J.; Hara, S.; Hiruma, K.; Fukui, T. Selective-Area Growth of III-V Nanowires and Their Applications. *J. Mater. Res.* **2011**, *26* (17), 2127–2141. https://doi.org/10.1557/jmr.2011.103.
(40) Johansson, J.; Wacaser, B. A.; Dick, K. A.; Seifert, W. Growth Related Aspects of Epitaxial Nanowires. *Nanotechnology* **2006**, *17* (11), S355. https://doi.org/10.1088/0957-4484/17/11/S21.
(41) Mariager, S. O.; Sørensen, C. B.; Aagesen, M.; Nygård, J.; Feidenhans'l, R.; Willmott, P. R. Facet Structure of GaAs Nanowires Grown by Molecular Beam Epitaxy. *Appl. Phys. Lett.* **2007**, *91* (8), 083106. https://doi.org/10.1063/1.2769401.
(42) Pankoke, V.; Kratzer, P.; Sakong, S. Calculation of the Diameter-Dependent Polytypism in GaAs Nanowires from an Atomic Motif Expansion of the Formation Energy. *Phys. Rev. B* **2011**, *84* (7), 075455. https://doi.org/10.1103/PhysRevB.84.075455.
(43) Jiang, N.; Wong-Leung, J.; Joyce, H. J.; Gao, Q.; Tan, H. H.; Jagadish, C. Understanding the True Shape of Au-Catalyzed GaAs Nanowires. *Nano Lett.* **2014**, *14* (10), 5865–5872. https://doi.org/10.1021/nl5027937.
(44) Jiang, N.; Joyce, H. J.; Parkinson, P.; Wong-Leung, J.; Tan, H. H.; Jagadish, C. Facet-Related Non-Uniform Photoluminescence in Passivated GaAs Nanowires. *Front. Chem.* **2020**, *8*.
(45) Pankoke, V.; Sakong, S.; Kratzer, P. Role of Sidewall Diffusion in GaAs Nanowire Growth: A First-Principles Study. *Phys. Rev. B* **2012**, *86* (8), 085425. https://doi.org/10.1103/PhysRevB.86.085425.
(46) Dubrovskii, V. G.; Sibirev, N. V. Growth Thermodynamics of Nanowires and Its Application to Polytypism of Zinc Blende III-V Nanowires. *Phys. Rev. B* **2008**, *77* (3), 035414. https://doi.org/10.1103/PhysRevB.77.035414.
(47) Caroff, P.; Dick, K. A.; Johansson, J.; Messing, M. E.; Deppert, K.; Samuelson, L. Controlled Polytypic and Twin-Plane Superlattices in Iii–v Nanowires. *Nat. Nanotechnol.* **2009**, *4* (1), 50–55. https://doi.org/10.1038/nnano.2008.359.
(48) Cantoro, M.; Brammertz, G.; Richard, O.; Bender, H.; Clemente, F.; Leys, M.; Degroote, S.; Caymax, M.; Heyns, M.; Gendt, S. D. Controlled III/V Nanowire Growth by Selective-Area Vapor-Phase Epitaxy. *J. Electrochem. Soc.* **2009**, *156* (11), H860. https://doi.org/10.1149/1.3222852.
(49) Spirkoska, D.; Arbiol, J.; Gustafsson, A.; Conesa-Boj, S.; Glas, F.; Zardo, I.; Heigoldt, M.; Gass, M. H.; Bleloch, A. L.; Estrade, S.; Kaniber, M.; Rossler, J.; Peiro, F.; Morante, J. R.; Abstreiter, G.; Samuelson, L.; Fontcuberta i Morral, A. Structural and Optical Properties of High Quality Zinc-Blende/Wurtzite

GaAs Nanowire Heterostructures. *Phys. Rev. B* **2009**, *80* (24), 245325. https://doi.org/10.1103/PhysRevB.80.245325.
(50) Shimamura, K.; Yuan, Z.; Shimojo, F.; Nakano, A. Effects of Twins on the Electronic Properties of GaAs. *Appl. Phys. Lett.* **2013**, *103* (2), 022105. https://doi.org/10.1063/1.4811746.
(51) Shapiro, J. N.; Lin, A.; Ratsch, C.; Huffaker, D. L. Temperature Dependence of Stacking Faults in Catalyst-Free GaAs Nanopillars. *Nanotechnology* **2013**, *24* (47), 475601. https://doi.org/10.1088/0957-4484/24/47/475601.
(52) Dubrovskii, V. G.; Glas, F. Vapor–Liquid–Solid Growth of Semiconductor Nanowires. In *Fundamental Properties of Semiconductor Nanowires*; Fukata, N., Rurali, R., Eds.; Springer: Singapore, 2021; pp 3–107. https://doi.org/10.1007/978-981-15-9050-4_1.
(53) Dubrovskii, V. G.; Sibirev, N. V. Growth Rate of a Crystal Facet of Arbitrary Size and Growth Kinetics of Vertical Nanowires. *Phys. Rev. E* **2004**, *70* (3), 031604. https://doi.org/10.1103/PhysRevE.70.031604.
(54) Cirlin, G. E.; Dubrovskii, V. G.; Sibirev, N. V.; Soshnikov, I. P.; Samsonenko, Yu. B.; Tonkikh, A. A.; Ustinov, V. M. The Diffusion Mechanism in the Formation of GaAs and AlGaAs Nanowhiskers during the Process of Molecular-Beam Epitaxy. *Semiconductors* **2005**, *39* (5), 557–564. https://doi.org/10.1134/1.1923565.
(55) Consonni, V.; Dubrovskii, V. G.; Trampert, A.; Geelhaar, L.; Riechert, H. Quantitative Description for the Growth Rate of Self-Induced GaN Nanowires. *Phys. Rev. B* **2012**, *85* (15), 155313. https://doi.org/10.1103/PhysRevB.85.155313.
(56) López, M.; Nomura, Y. Surface Diffusion Length of Ga Adatoms in Molecular-Beam Epitaxy on GaAs(100)–(110) Facet Structures. *J. Cryst. Growth* **1995**, *150*, 68–72. https://doi.org/10.1016/0022-0248(95)80182-C.
(57) *Arsenic Pressure Dependence of Surface Diffusion of Ga on Nonplanar GaAs Substrates - IOPscience*. https://iopscience.iop.org/article/10.1143/JJAP.33.11 (accessed 2023-04-05).
(58) Fedorov, V. V.; Dvoretckaia, L. N.; Kirilenko, D. A.; Mukhin, I. S.; Dubrovskii, V. G. Formation of Wurtzite Sections in Self-Catalyzed GaP Nanowires by Droplet Consumption. *Nanotechnology* **2021**, *32* (49), 495601. https://doi.org/10.1088/1361-6528/ac20fe.

For Table of Contents Use Only

The importance of As and Ga balance in achieving long GaAs nanowires by selective area epitaxy

Emmanuel Chereau[1], Vladimir G. Dubrovskii[2], Gabin Grégoire[1], Geoffrey Avit[1], Philipp Staudinger[3], Heinz Schmid[3], Catherine Bougerol[4], Pierre-Marie Coulon[5,6], Philip A. Shields[6], Agnès Trassoudaine[1], Evelyne Gil[1], Ray R. LaPierre[7], Yamina André[1]

[1]Université Clermont Auvergne, CNRS, Clermont Auvergne INP, Institut Pascal, F-63000 Clermont-Ferrand, France
[2]Faculty of Physics, St. Petersburg State University, Universitetskaya Embankment 13B, 199034 St. Petersburg, Russia
[3]IBM Research Europe - Zürich, Saumerstrasse 4, 8803 Rüschlikon, Switzerland
[4]Université Grenoble Alpes, CNRS, Institut Neel, 38000 Grenoble, France
[5]Université Côte d'Azur, CNRS, CRHEA, Rue Bernard Gregory, 06560 Valbonne, France
[6]Centre for Nanoscience and Nanotechnology & Department of Electronic and Electrical Engineering, University of Bath, Bath, BA2 7AY, United Kingdom
[7]Department of Engineering Physics, McMaster University, Hamilton, Ontario Canada, L8S4L7

TOC graphic

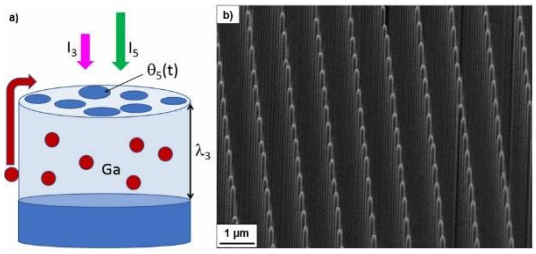

Synopsis

The growth of GaAs nanowires (NWs) on patterned SiN_x/GaAs(111)B substrate by hydride vapor phase epitaxy (HVPE) is demonstrated. A model was developed to describe the saturation of the NW lengths at high partial pressures of As_4, explained by the presence of As trimers. By decreasing As_4 partial pressure and hole size, high aspect ratio NWs were obtained.